Application of blue–green and ultraviolet micro-LEDs to biological imaging and detection

2008 J. Phys. D: Appl. Phys. 41 094013

(http://iopscience.iop.org/0022-3727/41/9/094013)

IOP PUBLISHING JOURNAL OF PHYSICS D: APPLIED PHYSICS

J. Phys. D: Appl. Phys. **41** (2008) 094013 (13pp) doi:10.1088/0022-3727/41/9/094013

INVITED PAPER

Application of blue–green and ultraviolet micro-LEDs to biological imaging and detection

H Xu[1], J Zhang[1], K M Davitt[2], Y-K Song[2] and A V Nurmikko[1,2]

[1] Department of Physics, Brown University, 184 Hope Street, Providence, RI 02912, USA
[2] Division of Engineering, Brown University, 184 Hope Street, Providence, RI 02912, USA

E-mail: Arto_Nurmikko@brown.edu (A V Nurmikko)

Received 3 December 2007, in final form 3 February 2008
Published 4 April 2008
Online at stacks.iop.org/JPhysD/41/094013

Abstract

This paper reviews authors' laboratory's work on the development of nitride-based blue–green and ultraviolet microscale LED devices with particular classes of imaging and spectroscopic applications in cellular level biology. Starting from neuroscience, we illustrate the utility of blue–green micro-LEDs for voltage-sensitive dye imaging of individual neural cells, as well as their ultraviolet counterparts for photostimulation of neurons. Arrays of micro-LEDs are also shown to be useful in projecting spatiotemporal patterns of photoexcitation to study the visual system development in living animals. As another illustration of the utility of the emerging nitride microdevice technology, we demonstrate the application of UV micro-LED arrays in bio-sensing technology as the core of a real-time fluorescence spectroscopy biowarning system.

(Some figures in this article are in colour only in the electronic version)

1. Introduction

Gallium-nitride based blue–green and UV LEDs have rapidly spurred a large space for optoelectronic applications, among which 'solid-state lighting' is perhaps the best example of an emerging high impact technology. To a lesser extent, the advances mean AlGaN LED device technology in the UV (from 340 to 280 nm) is replacing conventional UV lamp sources, also enriching applications ranging, for example from photochemistry to water purification and other biomedical purposes.

For most LED applications involving nitride LEDs, the active individual device areas tend to be fairly macroscopic, from around 100 μm^2 to over mm^2. On the other hand, pixelation for matrix addressable compact planar displays typically requires LED elements with diameters on the scale of 10–30 μm or so, introducing significant challenges in device microfabrication. The challenges derive in large measure from the combination of mechanical and chemical robustness of GaN, making it inherently difficult to craft complex device patterns with micrometre tolerances, to idiosyncratic electrical properties, including the typically insulating (sapphire) substrate. Nonetheless, progress has been made in establishing process flow protocols for micro-pixelation, as reflected by examples in this paper and elsewhere [1–5].

In this paper, we review device science research where microscale nitride LED sources have been applied to particular classes of imaging and spectroscopic applications in connection with cellular level biology. We concentrate mainly on work in the authors' laboratories and, in so doing, focus on two different types of application domains. First, we illustrate the utility of compact micro-LEDs in select problems in neuroscience, whereby individual neural cells can be fluorescently imaged by proximity illumination with blue–green LEDs, as well as phototriggered into electrical activity under targeted UV excitation. Arrays of micro-pixelated LEDs are also shown to be useful in projecting spatiotemporal patterns of photoexcitation to study visual neural pathways in a living animal (tadpole). Second, we show how the availability of new UV-based micro-LED arrays can be used to facilitate fluorescence based sensors, in a real-time fluorescence spectroscopy biowarning system, to alert

us regarding the potential presence of airborne pathogens in ambient environment.

2. Blue–green and UV micro-LEDs for neural imaging and stimulation

Imaging of biological structures at cellular level by photonic techniques is an advanced science and craft, most commonly applied in the context of fluorescently labelled probes that are excited by lasers or incoherent lamps within an integrated optical microscope-based imaging system. Dynamical events can be tracked, e.g. with fast CCD- or CMOS-based cameras and/or time resolved scanning laser imaging spectrometers with spatial resolution on the micrometre scale (and below as needed). Bright field, dark field, phase contrast and confocal techniques are just few of the microscope configurations used routinely.

Understanding of the growth and functionality of neural cells has been much advanced by these types of standard micro-imaging techniques, including the noninvasive recording of single neuron's electrical activity by probes such as cell-membrane infused voltage-sensitive fluorescence dyes (versus penetrating microelectrodes). However, the dependence of large incoherent lamp sources (or lasers) in the context of interfacing to microscope generally leads to rather bulky and expensive tabletop equipment. To enable greater flexibility of the illumination arrangements and with the aim towards compact, portable instrumentation, we have been increasingly adapting nitride-based LEDs in our laboratories as versatile sources of optical illumination and photoexcitation. In doing so, and in the absence of suitable commercial device sources, we have developed device fabrication processing techniques to produce micro-LEDs and their arrays that are tailored to particular imaging/photoexcitation configurations. Three examples of such device adaptation to specific neural cell studies are outlined next.

2.1. Blue–green micro-LEDs for dynamical imaging of neuronal circuitry

Access to detailed dynamical information of neural circuits is of basic interest to fundamental brain science as well as to efforts that aim to use such an insight to create new functional computational approaches for manmade devices. Typically, one is interested in the activity ('switching') of a single neural cell, as influences by adjacent interconnected neurons, i.e. a small circuit as the basic brain computational unit. In this section we demonstrate the utility of planar, compact LEDS for this purpose, by designing and fabricating small area ($<100\,\mu$m diameter) GaN based planar blue–green LEDs (both single element and array) as a flexible means to performing dynamical optical imaging of neurons, applied first cultured (i.e. 'dish-grown') hippocampal and cortical cells [6]. In particular, an individual LED can be aligned to illuminate a specific fluorescently labelled neural cell in close physical proximity. In addition, independent electrical control of each LED in the array with microsecond precision is achieved. The advantage of such an arrangement is particularly useful for neural cell networks that have been cultured on patterned periodic templates. Illumination of target neurons in a predetermined time sequence can then enable a new approach to dynamical recording of small patterned neural circuits. This approach is part of our longer term goal to develop a new type of dynamical imaging approach to neural networks, as well as to achieve an active 'chip-scale' interface between a neural and a manmade (optoelectronic) circuit.

The fluorescent tags which we used to label the neural cells in our experiments employed a membrane specific voltage-sensitive dye (VSD) stain, namely, the compound di-8-ANEPPS. The neural cell membrane potential-induced fluorescence change ($\Delta F/F$) of this dye can be maximized by employing a combination of excitation and emission filters that do not exactly correspond to the absorption and emission maxima of the dye. This is due to the voltage-dependent spectral shifts that accompany the absolute fluorescence amplitude changes caused by neural cell depolarization, once the cell 'fires' (i.e. transiently switches) [7]. The best signal-to-noise ratio with this dye ($\Delta F/F < 0.1$) was achieved by excitation in the green at ~530 nm and fluorescence collection above 570 nm, guiding the wavelength choice for our InGaN MQW micro-LEDs and their arrays.

2.1.1. Blue–green InGaN MQW LED device fabrication. The LED devices were fabricated from standard epitaxially grown p–n junction GaN heterostructure wafers (on sapphire), with an InGaN/GaN active multiple quantum-well region. A sacrificial silicon dioxide etch mask was patterned, and a chlorine-based reactive-ion etching (RIE) technique was used to etch the nitride to the n-type layer. A silicon dioxide passivation layer was deposited by plasma-enhanced chemical vapour deposition (PECVD). Arrays of p-contacts, which define the optical apertures, were created by electron beam evaporation of a multilayer Ni/Au (100/400 Å) metallization and lift-off technique. Several array geometries were used, with circular device apertures ranging in diameter from 25 to 200 μm and nearest neighbour edge-to-edge separation ranging between 25 and 150 μm. Ohmic contacts were created by standard multiplayer metallization and thermal annealing. Owing to large conductivity in the n-layer, a single n-electrode serviced several LED arrays in proximity. Finally, Ti/Au (100/1000 Å) pads were deposited in a layout that was convenient for electrical access and flip-chipping of the device onto a heat sink. Each element in the array had its own contact pad to make the LEDs to be individually addressable. Such arrangement enabled target illumination in any desired pattern or time sequence. The completed arrays were flip-chipped for light extraction through the polished sapphire backside (see figure 1). Using an epoxy die bonder, electrically conductive epoxy dots were deposited onto a suitably patterned silicon submount. For heat management and mechanical stability, thermally conductive, electrically insulating, epoxy was deposited in the area surrounding the optical apertures. Each chip containing three 3×2 arrays of devices was mounted onto a commercial DIP package for easy connection to the control circuitry and mounting under the microscope. The packaged LED is shown in figure 2(*a*), and the packaged LED array with one element ON is shown in figure 2(*b*).

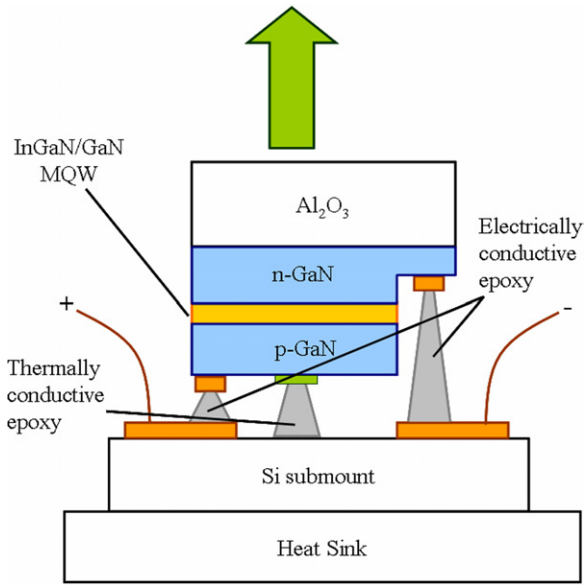

Figure 1. Schematic of flip-chipped InGaN blue–green LED mounting, showing basic device structure and main electrical contacts, including electrical and thermal epoxies.

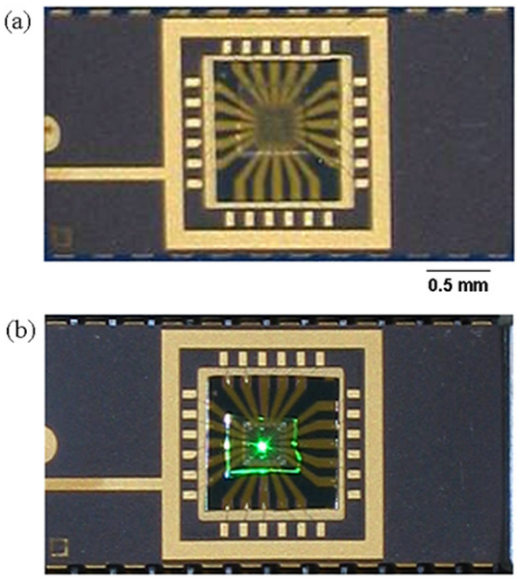

Figure 2. (*a*) Image of packaged LED array. (*b*) A single 50 μm diameter green device turned ON.

2.1.2. Dynamical imaging of neuronal circuitry. In these experiments, neural cells were grown in specific geometrical configurations, by patterning glass coverslips by lithographic techniques with molecular monolayers of poly-L-lysine acting as local biocompatible 'adhesive' to anchor the cells at a selected location during incubation. The culturing techniques followed procedures established earlier for culturing of hippocampal neurons, extracted in our case from embryonic day 18 (E18) rat embryos. Cells were plated onto poly-L-lysine coated glass coverslips at a density of 5000 to 10000 cells cm^{-2}. Cultures were subsequently fed every four days until use in the optical experiments [8]. When used, the neural cells were stained for 10 min by bath application of 20 μm di-8-ANEPPS in the saline bath [6].

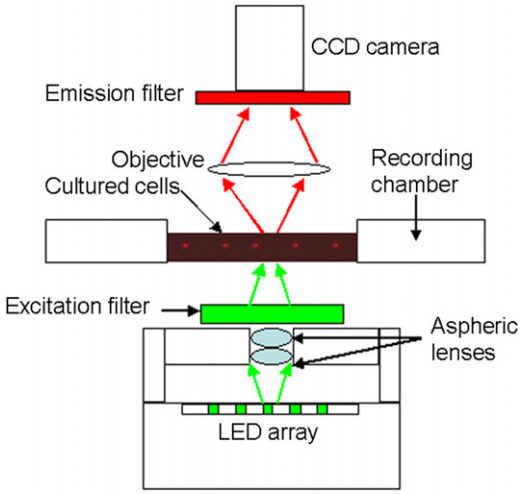

Figure 3. Schematic of optical setup for targeted single (cultured) neural cell illumination by bottom illuminated green micro-LED array.

A schematic of the LED-based fluorescence imaging test arrangement is shown in figure 3. A pair of aspheric lenses (f = 5.95 mm, F-number = 0.88) was used to collect light from the LEDs with a bandpass filter to eliminate the long wavelength spectral tail of the LED emission (one disadvantage in using LEDs for as excitation sources in general). The LED assembly was placed below the thin fluidic vessel housing the cultured cells (a perfusion chamber), to enable focusing of the photoexcitation onto single cells (body diameter ~20 μm) with bottom illumination. By carefully choosing the properties of focusing optics, we could achieve one-to-one focusing. The fluorescence emission from the VSD labelled cells was collected upwards by a 40× microscope objective with a proper choice of dichroic and emission filters and was projected onto a high speed CCD imaging camera. An ultralow-noise current source was manually connected and supplied current to the chosen LED elements and was modulated to control the on–off timing of the LEDs. In parallel, and for validating the all-optical approach, the electrical activity of the neural cells was also recorded by membrane penetrating microelectrodes, typical of such invasive electrophysiological techniques (whole-cell patch clamp recordings) [9, 10]. After cell staining, the condenser of the Nikon E600FN microscope, which was mounted on a manipulator, was positioned and made to illuminate the cells for conventional differential image contrast (DIC) viewing to facilitate LED alignment. A particular cell was chosen, and an LED from the array was brought under the cell of interest. Fluorescence data were then acquired at 1 kHz using an 80 × 80 element CCD imaging camera.

A representative example of results obtained using the above-described LED-based excitation scheme is shown in figure 4 with a single cell-targeting LED device operating at 60 mA (corresponding to ~0.16 mW output power) current for a time window of 250 ms. The top trace shows the electrical signal recorded intracellularly (invasively), displaying 'action potential' spikes, whereas the bottom trace shows the optically derived signal corresponding to modulation in fluorescence

amplitude of the VSD. The action potential spikes were triggered by a stimulus voltage pulse applied to the cell-embracing electrolytic (saline) solution. The optical signal corresponds to an approximately 4% change in fluorescence intensity for the ∼100 mV action potential.

With this type of new capability offered by the ability of applying individual LED illumination onto specific neurons in a patterned cellular network, with the advantage of being able to manipulate the pattern and time sequence of illumination, we can envision the use of these micro-LED arrays with pixel-size matched/imaged photodiode arrays for dynamical optical recording of the activity of multiple neural cells, eventually extending to an entire neuronal circuitry on a chip-scale device. An initial example of this is shown in figure 5 for the case of two adjacent neurons in a cellular network. Figure 5(*a*) shows the DIC microscope image of two such interconnected hippocampal cells. In figure 5(*b*), two LED elements have been used to illuminate the two chosen cells. Figure 5(*c*) shows a series of fluorescent images of the two cells, when both LEDs are first turned on simultaneously and when each LED is turned on separately during a chosen time interval. Figure 5(*d*) shows a concept schematic of the chip-scale optical recording system. By rapid electrically directed scanning of the LED arrays, neurons in their microcircuitry will be illuminated sequentially with fluorescent signals being detected by the corresponding photodiode elements. Neither microscope nor fast imaging (CCD/CMOS) camera would be needed for such a system.

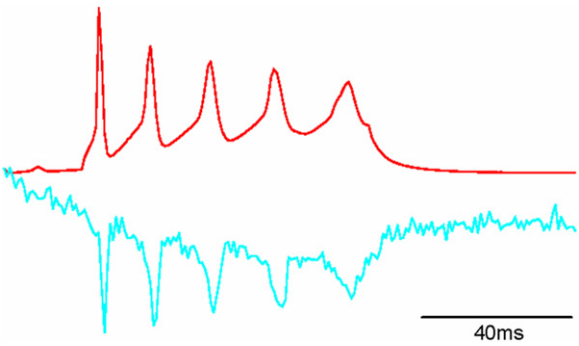

Figure 4. Top: electrical signal from hippocampal neuron. Bottom: optical signal using LED as excitation source.

2.2. UV micro-LEDs for activation of electrical response in neural cells by photochemical flash photolysis

Flash photolysis techniques have been successfully used for photoinducing biochemical events across different neuronal preparations, thereby allowing the complex neural signal integration process to be studied in detail. This technique involves UV-catalyzed photocleaving caged precursors for release of compounds that provide a physiological trigger to a neural cell, such as calcium ion, neurotransmitters, fluochromes, peptides and enzymes, [11]. The light source used in these experiments must deliver high intensity UV irradiation (typically in the wavelength range 300–380 nm) in order to ensure adequate photocatalysis of the inactive species to the active form. Arc lamps and large frame bench-top lasers, currently used in such photolysis studies, are either coupled directly to microscopes or coupled via fibres to deliver

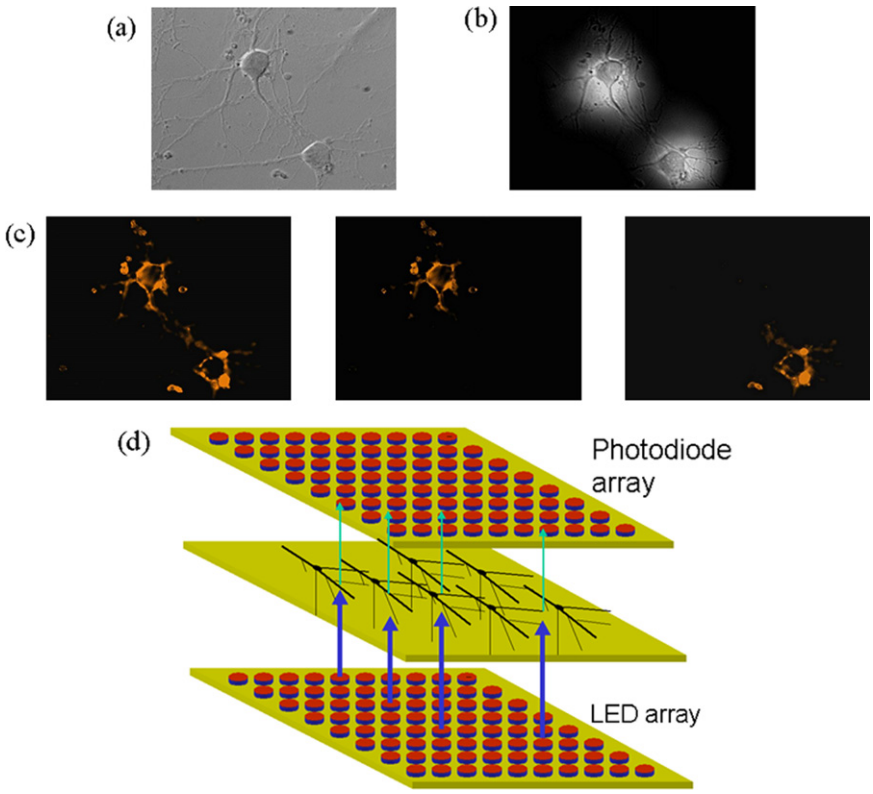

Figure 5. (*a*) Microscope image of hippocampal neural cells in culture (differential contrast mode). (*b*) Two individual elements of the micro-LED array elements located under two neighbouring cells. (*c*) Fluorescent images when both illuminating LEDs are turned ON, and one is ON at a given gated time, respectively. (*d*) A concept schematic of the chip-scale optical recording system.

UV pulses to the biological samples [12–14]. Especially in the UV, such sources tend to be bulky and expensive, often requiring complex focusing optics. In contrast, the newly emerging compact AlGaInN-based UV LEDs, emitting in the 280 and 340 nm wavelength ranges with relatively high output power and operating speeds, provide viable alternatives that are compact and inexpensive, yet high intensity sources when configured appropriately [15, 16].

In this section we highlight the use of custom-designed and fabricated nitride UV micro-LEDs as a practical means to performing flash photolysis of caged neurotransmitters and subsequent triggering of neural cell activity [17]. We have designed and fabricated small area planar UV LEDs (<100 μm diameter) in which individual LED elements can be aligned to illuminate a specific hippocampal neural cell in close physical proximity, so far *in vitro*. Careful positioning of the UV element to illuminate specific regions in the cultured hippocampal cell in proximity allows for precise quantitative control over the release of neurotransmitter. In the experiments reviewed next, the neural cell preparations were quite similar to the cell cultures (described in the previous section), but with sapphire substrates (Meller Optics) replacing the glass substrate so as to achieve high transmission rate in the UV range for bottom illumination by micro-LEDs. The overall device fabrication strategy was dictated by the desire to effectively integrate the micro-LEDs onto a compact neural cell study platform for targeted proximity illumination, as opposed to the 'long' distance source-to-target geometry typically employed in conventional flash photolysis experiments.

2.2.1. Ultraviolet AlGaN MQW LED device fabrication. The wavelength of the UV LEDs was chosen to be near 340 nm, to match the maximum absorption of a DMNB-caged glutamate [17]. The 34 nm wavelength LEDs were fabricated from MOCVD-grown quaternary AlGaInN quantum-well p–n junction heterostructures [18], according to a material design typical for these compact solid-state light emitters. As the sapphire substrates are transparent at this wavelength, the light emission could be extracted from the polished backside through the 500 μm thick substrate. A summary of the device fabrication process flow was as follows: mesa-type LEDs were etched using chlorine-based RIE and a high-temperature (850 °C for 1 min) annealed multilayer Ti/Pd/Al/Ti/Au metallization (by photolithography and electron beam deposition) served as the contact to n-type AlGaN [19]. An opaque Ni/Au (100/400 Å) p electrode annealing at 600 °C for 5 min, 50 μm in diameter, defined the optical aperture, as illustrated in the inset of figure 6(*a*). In contrast to longer wavelength blue and green InGaN LEDs, 340 nm devices have lower n-type conductivity and require n and p contacts which are laterally closer to the active region for high conversion efficiency. In our devices, the lateral n to p distance was on the order of 20 μm, eliminating so-called current crowding effects, which can reduce the efficiency of larger area devices, particularly in sub-300 nm wavelength devices. The device emission spectra and typical light output power and current–voltage characteristics of fully fabricated individual 50 μm diameter (optical aperture), 340 nm emitting micro-LEDs are shown in figure 6(*b*).

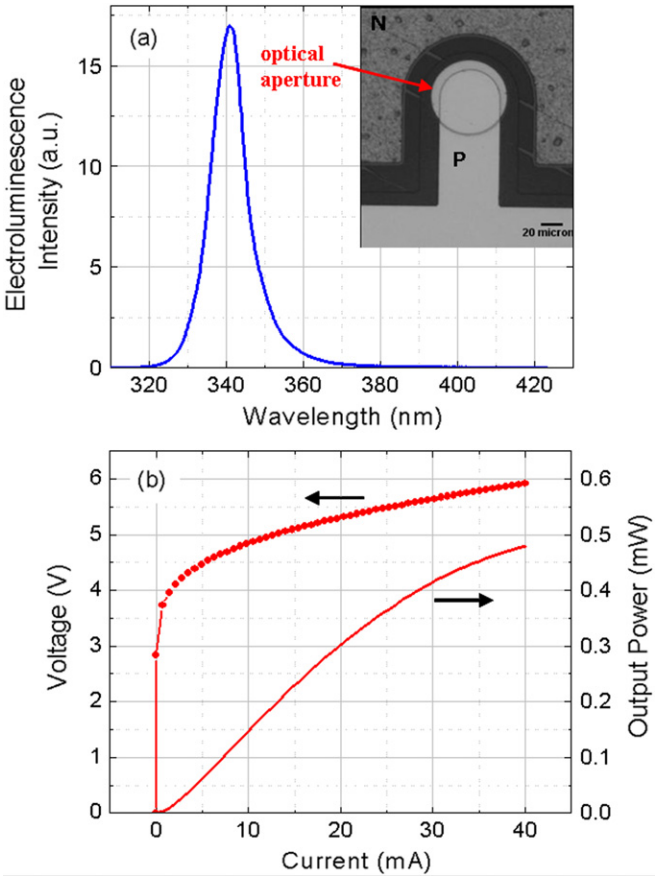

Figure 6. (*a*) Electroluminescence spectrum and (*b*) typical dc light-output (measured through the transparent sapphire substrate using a UV-enhanced silicon photodiode (Hamamatsu) placed in close proximity to the backside of the device) and current–voltage characteristics for a 50 μm diameter 340 nm LED. Inset: photographic image of single device.

2.2.2. Experimental setup. The integrated experimental setup was constructed as follows. The UV micro-LEDs were mounted on a copper ring for thermal management and inserted into a 1 inch mirror mount for easy handling. The backside illuminated device offers the advantage of removing the electrical wiring from the optical path thereby allowing the LEDs to be placed in close proximity to the cultured neuron substrate. A pair of fused silica aspheric lenses with appropriate focal lengths was used to focus the UV light onto the sample and the entire assembly was mounted on a custom built holder and placed below the chamber containing the cultured cells (figure 7). A tight focal spot (~50 μm) imaged from a single 50 μm device was achieved (see figure 9(*a*)). In order to monitor the cellular activity, we again employed the so-called whole-cell patch clamp recordings which were performed using the same instruments and solutions as in section 2.1. The cultures were studied at room temperature (27 °C) after 1 week *in vitro*. The patch pipettes were made of borosilicate glass and had a resistance of 3–4 MΩ when filled with the pipette solution. The delivery of the caged glutamate was applied locally near individual neural cells by using a micropipette under pulsed positive pressure (referred to as the 'puffer pipette'). The puffer pipette was connected to

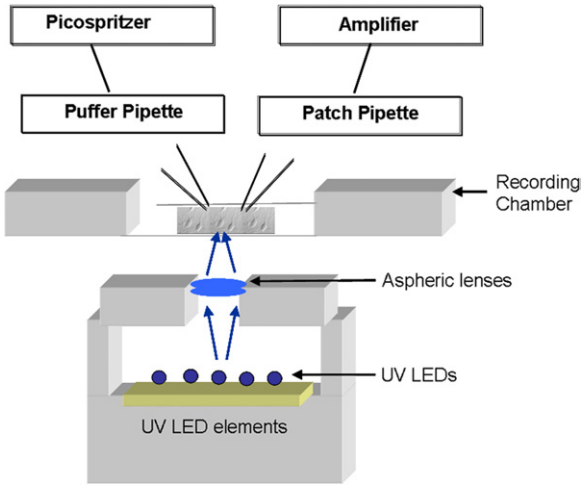

Figure 7. Schematic showing the setup: individual LED elements are focused onto neural cells using a pair of aspheric lenses; the entire assembly is mounted on a custom built holder that can be positioned under the neural cell of interest.

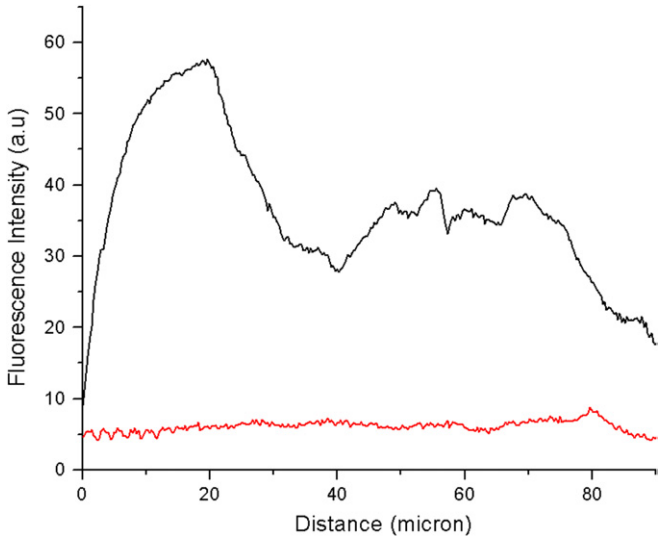

Figure 8. Fluorescent intensity before (upper trace) and after (lower trace) illuminating caged-FITC sample with UV light from a 50 μm LED device.

a 'picospritzer' unit, which applied controlled pressure pulses releasing precise amounts of solution into the medium.

In order to test the viability of the micro-LEDs to efficiently UV 'uncage' molecules by flash photolysis, we first used as a reference material a caged version of a fluorescent label, caged-FITC (CMNB-caged Fluorescein, molecular probes) dissolved in water. Fluorescent images of a thin liquid film of caged-FITC before and after UV irradiation were captured. Figure 8 shows the fluorescent intensity as a function of distance with the red trace representing the FITC fluorescence before UV irradiation while the black trace shows the intensity from the same region after illuminating with UV light from a 50 μm LED element for 1 s. (The varying intensity peaks in the black trace correspond to irregularities in the substrate.) Integrating the area under these curves we obtain an approximately 3-fold increase in fluorescence intensity, implying that the light from the UV LED is efficiently breaking the chemical bonds of the molecular cage, and hence releasing/activating fluorescein.

2.2.3. UV-uncaging of caged glutamate. The capability of UV LEDs to uncage neurotransmitter and activate proximate individual hippocampal cultured cells was tested as shown in figure 9(*a*) which displays an image of a single hippocampal neuron indicating the positions of both the recording patch and the puffer micropipettes delivering caged glutamate. The entire LED assembly with the corresponding focusing optics was mounted on a 3D stage that allowed for precise positioning of the LED element below the region of interest. Whole-cell recordings were made on a given neuron; the cellular 'action potential' switching events were triggered by injecting current through the patch pipette at the beginning of the experiment, but thereafter this pipette was used only to record the electrical activity of the cell. The timing and delay of the picospritzer and LED circuit were carefully and independently controlled, while individual micro-LEDs were typically operated between 30 and 55 mA drive current (translating to 0.4 mW output power) for 250–350 ms pulses. During these experiments, the picospritzer was typically regulated at a pressure between 6 and 20 psi for 20–200 ms. Control experiments are shown in figures 9(*b*) and (*c*) as the response of the neuron to only the LED being ON and only the puffer being ON, respectively. In neither case was there an indication of induced neural activity, showing that neither the LED nor the caged glutamate triggers any neural response from the cells on its own. However, with both the puffer and the LED turned ON (ON times indicated by the red and blue traces), we could readily observe neural cell electrical switching, as shown from the recordings from two cells in figures 9(*d*) and (*e*). The ability to trigger action potentials in the neuron indicates that the UV LED effectively uncaged the glutamate that was delivered in the immediate vicinity of the neuron, providing the neurotransmitter excitation action. (It is also clear from figures 9(*d*) and (*e*) that by carefully controlling the picospritzer conditions, it is possible to achieve shorter latencies between the beginning of depolarization and the firing of action potential.) Experiments such as these hence show graphically the utility of nitride UV micro-LEDs as efficient and effective sources for flash photolysis experiments simplifying and reducing the cost and size of conventional setups that require expensive and complicated instrumentation.

2.3. Combining multicore imaging fibre with matrix addressable blue/green led arrays for spatiotemporal photonic excitation in the research of visual system development

In this section we describe the development of an integrated multi-element micro-LED and endoscopic imaging system, to enable portable means of projecting spatiotemporal patterned photoexcitation in biomedical applications. We describe the LED array design and fabrication strategy in some detail and then proceed to a specific demonstration application which involves in our study the early development of the visual system in a simple but useful animal, namely, a tadpole.

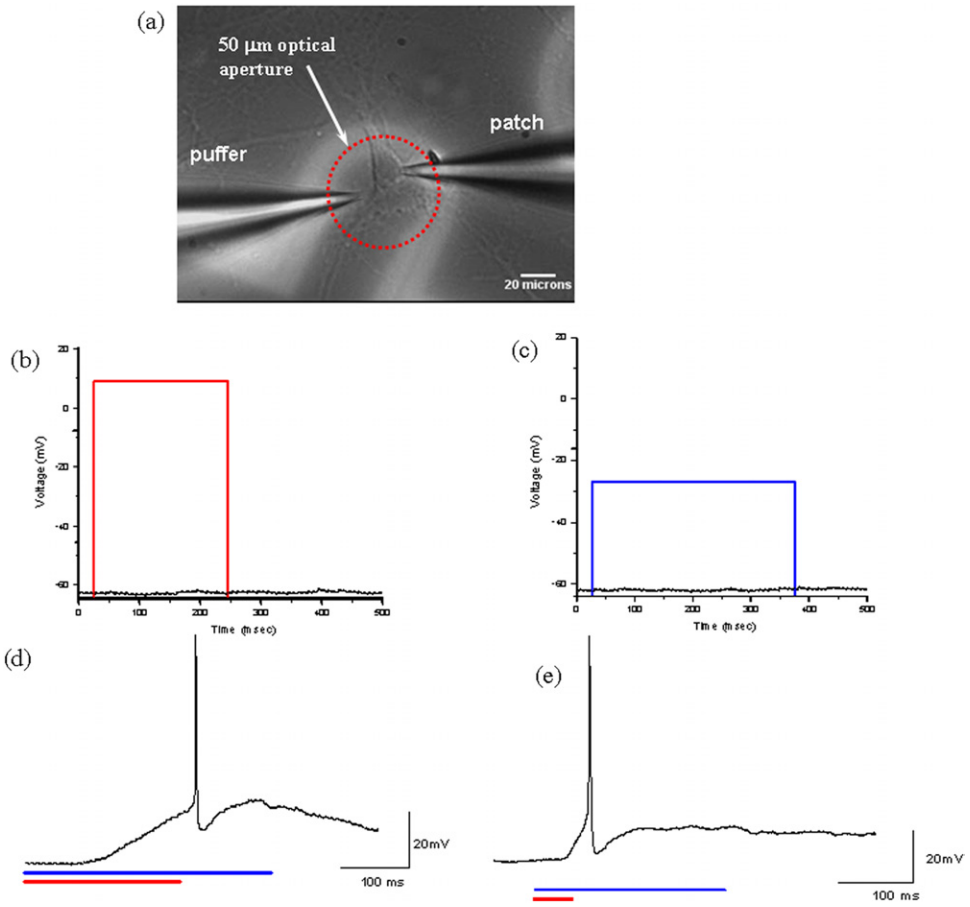

Figure 9. (*a*) Image of the neuron with corresponding puffer (left) and patch (right) pipettes, (*b*) control experiment with the puffer: red (square) trace indicating the duration of puffer pulse, black trace shows the cell's response, (*c*) control experiment with the LED; blue (square) trace indicating the duration for which LED is ON, black trace shows the cell's response, and ((*d*) and (*e*)) response recorded from two different cells when both the puffer (red, lower lines) and LED (blue, upper lines) were ON. (Colour online.)

The development of neural circuits is significantly regulated by neural activity in the visual system, where the onset of patterned visual activity has been shown to lead to refinement of inputs to a number of visual areas in the vertebrate brain. For amphibians, such as the tadpole, the 'optic tectum' is the primary visual information processing area in the brain and receives a topographically well-organized projection from retinal receptors ('photodetectors'), resulting in progressive refinement and eventual stabilization of the retinotopic map by adulthood. Thus having an *in vivo* simple image projection system is a valuable tool in such developmental studies.

2.3.1. Blue/green LED array fabrication and image fibre coupling. The key element of our microscale flexible optical image projection system is the integration of a 100 element InGaN MQW blue/green two-dimensional (2D) LED array with a multicore imaging fibre [20]. A system level schematic of the system is shown in figure 10, where a scalable matrix addressing scheme enabled electrical access to individual elements in the densely packed 2D-LED array. In devising the fabrication strategy for the LED microarray, we needed to innovate several process steps to craft a matrix addressable array from otherwise relatively standard blue or green LED wafer level starting material. The prototype LED array device

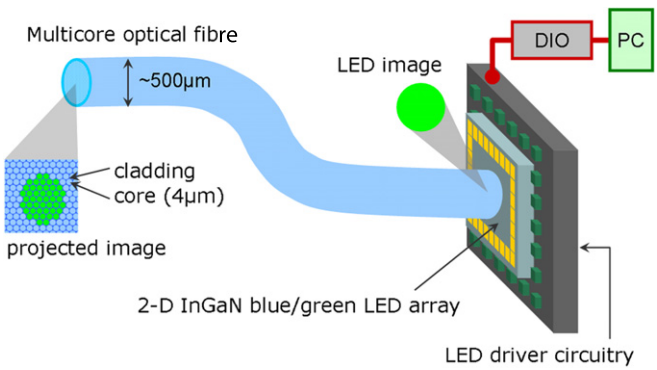

Figure 10. Overview of an integrated 100 element blue–green LED array-driven flexible fibre optic image projection system.

consists of 100 emitter pixel elements within the 500 μm^2 area, with a 28 μm diameter for an individual element in the array and 50 μm centre-to-centre spacing for neighbouring elements. A process flow diagram is shown in figure 11. A nickel based multilayer etch mask was first formed on top of the wafer material using photolithography patterning and electron beam evaporation, followed by a lift-off process. The wafer material was then deep-etched (>5 μm, down to the sapphire substrate) using chlorine-based RIE in order to form

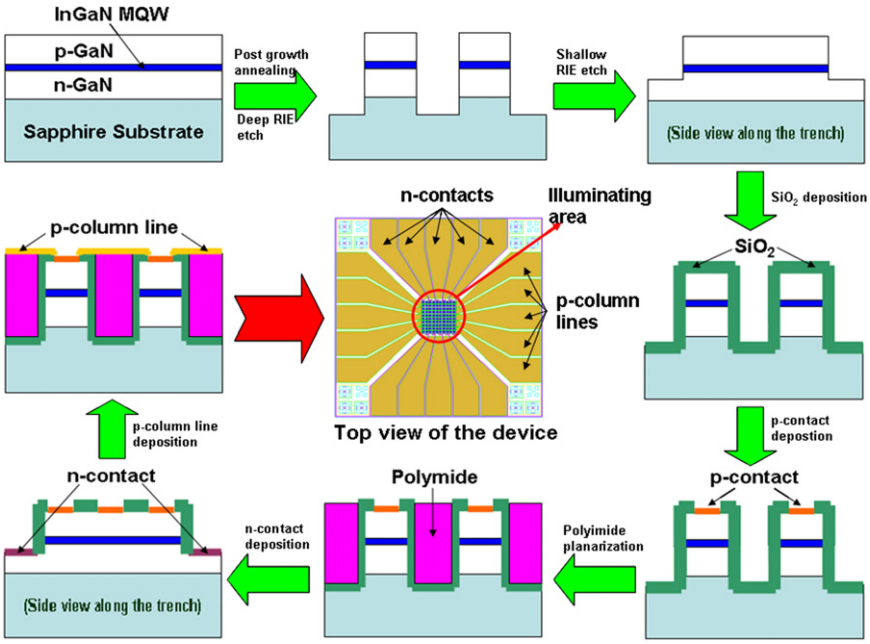

Figure 11. Schematic of the fabrication process flow of a 10 × 10 LED microarray (see text for details).

row trenches for electrical isolation. A shallow-etch followed, using the same etching technique and a conventional silicon dioxide etch mask (formed by using PECVD silicon dioxide deposition, photolithography patterning and 5% buffer HF wet etch) to expose the n-contact layer, which were shared by LED elements on the same rows. Next, a semitransparent p-contact deposition (Ni/Au: 50 Å/50 Å) on the aperture was achieved by electron beam evaporation after SiO_2 passivation and photolithography patterning. Thermal annealing at 600 °C for 5 min followed to form an ohmic contact. In order to create cross-trench column lines, a planarization procedure was employed before further processing. Thick layers of polyimide (PI-2771 from HD MicroSystems) were deposited by spin coating, cured at 350 °C for 1 h, and subsequently etched back with oxygen plasma several times to reveal rows of semiconductor surfaces with polyimide filled trenches in between. This step was repeated several times in conjunction with AFM scans of the surface morphology, to ensure that the trench depth (after planarization) was no greater than 2000 Å. Finally, n contacts (Ti/Al/Ti/Au: 100 Å/600 Å/100 Å/800 Å) and p-column lines (Ti/Au: 100 Å/1000 Å) were patterned and deposited by standard photolithography and electron beam evaporation. Shown in figure 12 are the performance characteristics of a typical individual 'pixel' emitter element in an array. In the 'LIV' traces, both the light output power density and voltage are plotted as a function of the current density. Low turn-on voltages (especially for green devices) and robustness of the device under high current injection were obtained from both blue and green devices across the arrays. Due to finite conductivity of GaN, there is an approximately 25 Ω sheet resistance difference for neighbouring elements in the same row within the array. We resolved this imbalance by correcting it in the drive electronics so that the turn-on voltages and light outputs of different elements became quite uniform (<5%) across the arrays.

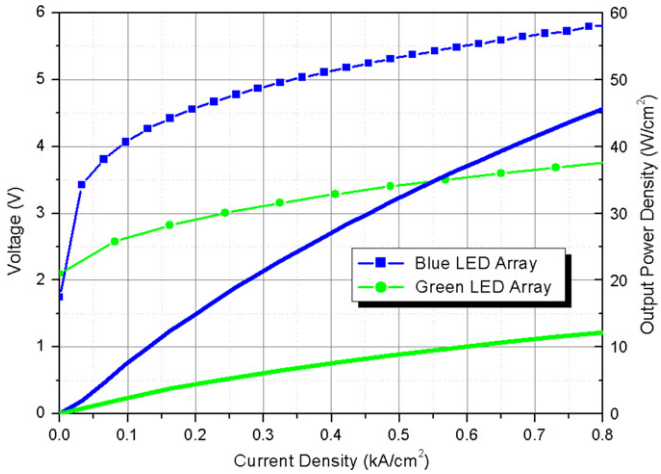

Figure 12. The 'LIV' curves of an individual element in the matrix addressable blue and green LED arrays (prior to coupling to imaging fibre).

The nitride LED microarrays were optically connected (butt-coupled, coupling efficiency ∼4%) to a 3-foot long 30 000 pixel multicore image fibre (FIGH-30-650S from Fujikura Ltd) of 600 μm image area diameter with 1.9 μm individual pixel diameter and 3.3 μm intercore distance to guide light from the LED array. Various high resolution imaging techniques based on multicore fibres have been reported by several groups [21–23], indicating good image quality and low crosstalk. A spatiotemporal pattern of light with 96 elements (4 corner elements cannot be coupled due to the size of the fibre) at the output end of the fibre was observed (see figure 13). To drive the LED arrays, we designed and built a matrix addressable control circuit that connects to a DIO card (DIO-Card-6534, from National Instruments) to drive the device. The whole system was controlled via a Labview program on a computer. Two scanning modes were

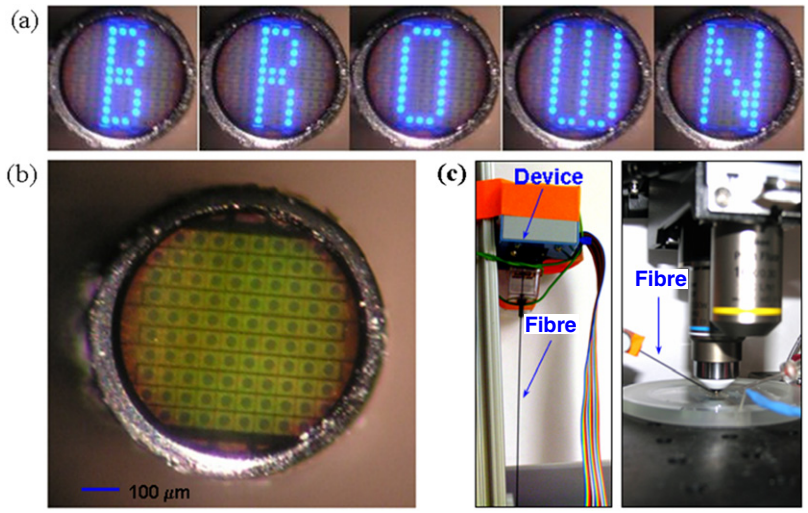

Figure 13. (*a*) Emission patterns generated at the end of the multicore image fibre. (*b*) An image of the blue 10 × 10 LED array projected through the image fibre (turned off). (*c*) Images of the packaged device and a close-up of the fibre end on the setup.

available for controlling the arrays: (i) line mode (in which elements are accessed row by row) and (ii) pixel mode (in which elements are accessed one by one). The maximum scanning rate of a pattern was 10 kHz, which is sufficient for a broad range of biomedical applications in providing high speed spatiotemporal photoexcitation patterns.

2.3.2. Photostimulation of retinal ganglion cells for visual system development studies. In an illustrative application experiment, our 10 × 10 matrix addressable LED array has been used to deliver patterned visual stimuli directly onto the retina of developing (Nieuwkoop and Faber, developmental stage 48) *Xenopus laevis* tadpoles (see figure 14(*a*)). This animal is a useful and practical testbed for the study of retinotopic mapping due to easy optical access to the eyes as well as recording access to the brain. The retinal sensitivity is especially pronounced in this animal in the blue–green region of the spectrum. In our experiments, the response of optic tectal neurons in the tadpole brain was probed electrically via a standard electrophysiological patch clamp microelectrode technique, under different light excitation patterns from the microscale flexible LED array driven device, in order to map the so-called visual receptive field (i.e. a single neuron's response to stimulations from different retinal areas) of tectal neurons (see figure 14(*b*)). By doing so, we could measure the degree of convergence of retinal inputs into a given tectal cell. This was done at different developmental stages to study the formation of the retinotopic map during development of the visual system. While not relevant here, the details of these neuroscientifically meaningful new results will be published elsewhere. Additionally, we note that we have been able to apply direct optical stimulation of the brain as well (with finite optical absorption by neural cells in the blue) to elicit some neural response. In summary, these experiments show the utility of the blue (and green) LED microarrays, integrated with the imaging optical fibre, as a flexible and compact optoelectronic tool for all types of photoexcitation schemes where portability and compactness have a premium value.

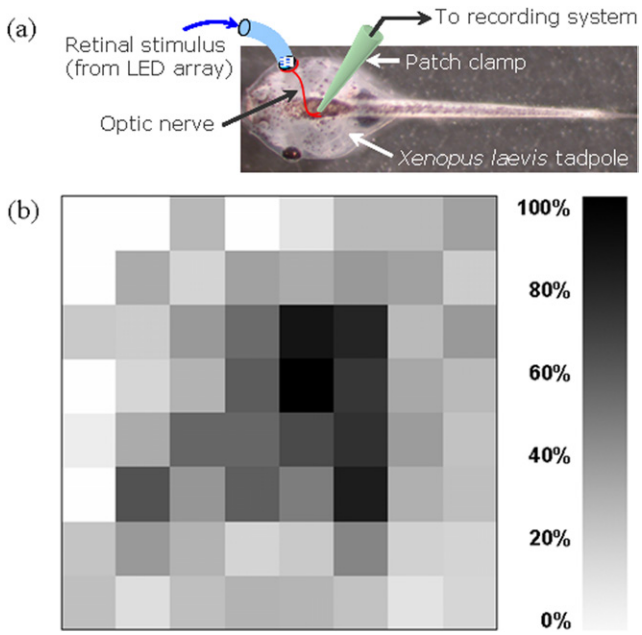

Figure 14. (*a*) Schematic of the matrix addressable LED array retinal stimulation with tadpole optic tectal neuron recording using a patch clamp. (*b*) A grey scale of the visual field response map of an optic tectal neuron of a tadpole to individual LEDs driven CW across the central 8 × 8 output of the fibre coupled array. Each square represents a LED element. Different grey scales refer to different response strengths; e.g. a black block means the probability of getting response from the neuron when you turn on the LED at this position is 100%. The excitation patterns from the fibre end, which was fixed very close to the tadpole's eye (within a few millimeters), were imaged on the retina via the tadpole's own eye lens.

3. UV micro-LED arrays for bio-sensing of aerosols

In this section, we highlight the utility of nitride-based micro-LED arrays in a very different application area, namely to provide information regarding the potential presence of airborne pathogens in the ambient environment. Specifically, we show how compact UV sources can be used to facilitate

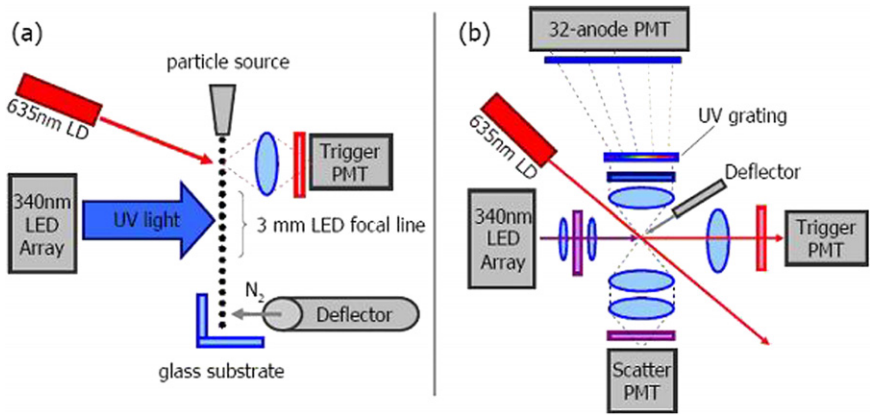

Figure 15. Schematic of core optical system showing placement of aerodynamic deflector and substrate for sample collection. (*a*) Front view and (*b*) top view.

fluorescence-based sensors, in a real-time fluorescence spectroscopy biowarning system.

Ultraviolet laser-induced fluorescence is a technique that has long been used in bio-aerosol particle detectors [24]. Recent advances in device performance has prompted interest in UV LEDs at 290 and 340 nm, key wavelengths of excitation for intrinsic bio-fluorescence, as potential alternative sources of UV excitation over solid-state lasers. Jeys *et al* [25] have investigated the use of dual-wavelength, single element LEDs, and Davitt *et al* [26] have demonstrated a compact system operating with a linear array of UV LEDs. In keeping with miniaturization of the UV source and design of a compact spectrometer for on-the-fly fluorescence analysis of single airborne particles in this work, we present an optical system with an integrated miniature aerodynamic deflector to separate and concentrate particles with interesting or suspicious fluorescence spectra [27]. Custom electronics has been developed to manage a standalone system and accomplish real-time processing of optical data. Although the demonstration reviewed here uses aerosolized particles, the LED array excitation source, compact spectrometer, real-time electronics and particle deflector in particular are portable in aqueous environments in general.

The nitride UV LED microarray-based aerosol particle sensor system is designed with the primary objective of making a real-time and compact front-end sensor able to classify particles by fluorescence spectra and physically sort a subset of particles from the background. In this demonstration we use fluorescent polystyrene latex spheres (PSLs) as test particles for sorting purposes. In the bio-aerosol detection application, a front-end sensor is one that can rapidly sort a sample of particles from the ambient and provide an early warning signal if potentially suspicious particles are present. Thus, it need not have microbiological-level specificity in identifying threats, but instead serves as a trigger to subsequent analyses which take significantly longer time, up to hours, but have better identification capabilities.

3.1. All-optical aerosol sensing system

The overall design of the all-optical aerosol sensor is shown schematically in figure 15 including the location of the 'suspect-particle-sorting' mini-aerodynamic deflector, all of which is contained within a footprint of $25 \times 35\,\mathrm{cm}^2$. The proof-of-concept optical apparatus and UV LED light source design have been described in detail previously [26]. Briefly, particles ejected from the nozzle travel in a laminar jetstream for approximately 1 cm and travel at a velocity of approximately $2\,\mathrm{m\,s}^{-1}$. Immediately upon exiting the nozzle, particles pass through the focused spot of a 635 nm laser diode (LD). The scattering signal, detected by a photomultiplier tube (PMT) equipped with a red bandpass filter, is used as the trigger signal to control the timing for the subsequent events. Each particle passes through the focal plane of the UV LED array during which time the fluorescence spectrum is collected by a compact spectrometer consisting of a collection lens, transmission grating, filter and 32-anode PMT; scatter intensity is collected simultaneously. This arrangement collects spectra spanning 325–700 nm in 32 equally spaced bins. The UV illumination source is a linear array of 32 independently addressable LEDs oriented vertically such that sequential flashing of the LED elements at a rate matched to the average particle velocity in the jetstream results in tracking the particle over a vertical distance of approximately 3 mm. A linear array of individual UV LEDs offers several advantages over a single element illumination source; first, an increase in the total energy delivered to the particle, which is achieved both by extending the excitation time as well as enabling the use of higher injection currents, and second, a reduction in the background elastically scattered signal.

The 290 nm or 340 nm emitting LEDs are fabricated from MOCVD-grown AlGaN and AlGaInN quantum-well p–n junction heterostructures whose growth represents significant challenges in device science. Details of epitaxial growth, structure, process conditions and device characterization are given in Ren *et al* [18]. Illustration of state of the art in UV LED development can be found, for example, in Adivarahan *et al* [28] and references therein. Currently semiconductor UV emitters have lower output powers than other UV sources; however their geometry can be tailored specifically to the task and have significantly reduced size and cost advantages over traditional LIF systems employing solid-state lasers.

Other features of the all-optical sensor system include a timing control implementation, which requires a sequence

of timed events and was entirely accomplished with three electronic boards designed (for this purpose for details, see [19]). Finally, after fluorescence-based spectral real-time indication, our system also featured a solenoid-based aerodynamic deflector whose role was to separate 'suspect' particles by short horizontal bursts of nitrogen gas. Deflected particles were collected onto a glass substrate made from microscope coverslips, which is placed 2 mm below the deflector nozzle. (Deflected particles are deposited onto the vertical portion of the substrate while the undeflected jetstream accumulates on the horizontal glass.)

3.2. *UV induced fluorescence detection of microparticles*

For system demonstration, dye-filled PSLs were used as simulants of bio-fluorescence. Two types of PSLs were used, 1 μm diameter blue fluorescing (Molecular Probes, F8815) and 2 μm green fluorescing (Duke Scientific, XPR-801). In this case, both are readily excited by 340 nm light (though we have also incorporated 280 nm UV LED arrays into the system). This is also a key wavelength of excitation for intrinsic bio-fluorescence, attributed broadly to NADH. The spheres are diluted to known concentrations in water and the solution is then ejected in 70 μm diameter droplets at a rate of 10 Hz by a piezo-electric generator (MicroDrop GmbH). The concentrations are chosen such that the particles consist of water with statistically less than 1 PSL per drop. For the results shown in figure 16, the drive current pulse per element was a modest 20 mA for a duration of 53 μs corresponding to 0.3 mW output power per element at the source. Figure 16(*a*) shows a portion of the PC display that shows the UV scatter intensity detected per element of the LED array. Intensity differences over the 32 LEDs are due to imaging optics, which contribute to centre elements being better focused and to element-to-element variation in device characteristics. Figure 16(*b*) summarizes a series of demonstrations. Either blue–doped or green-doped PSLs were separately passed through the system and a simple one-spectral-band algorithm was used to evaluate whether a particle was present or not. In this case, a flag to the deflector was generated upon the condition that the average charge collected over a 35 nm wide spectral range centred about the peak fluorescence (525 nm and 435 nm for the green and blue PSLs, respectively) was greater than a threshold level of 1 pC. The threshold was chosen to lie above the background level—due to detector noise and stray LD light—of roughly 10 photons per PMT channel accumulated during the total 1.6 ms fluorescence collection time, the time during which the particle traverses the LED array focal line. Shown in figure 16(*b*) are the average fluorescence spectra of flagged events during a test of 5000 particles; commensurate with the PSL concentration, nearly 200 particles were flagged to create each plot. A solution containing a mixture of both types of PSLs was tested, statistically approximately 0.1 green and 0.05 blue PSL spheres per drop, and a one-band algorithm to isolate the green particles was applied. In addition, a two-band algorithm where the same wavelength bands were used but where a flag was generated only upon the Boolean condition (green = true) AND (blue = false) was used in order to

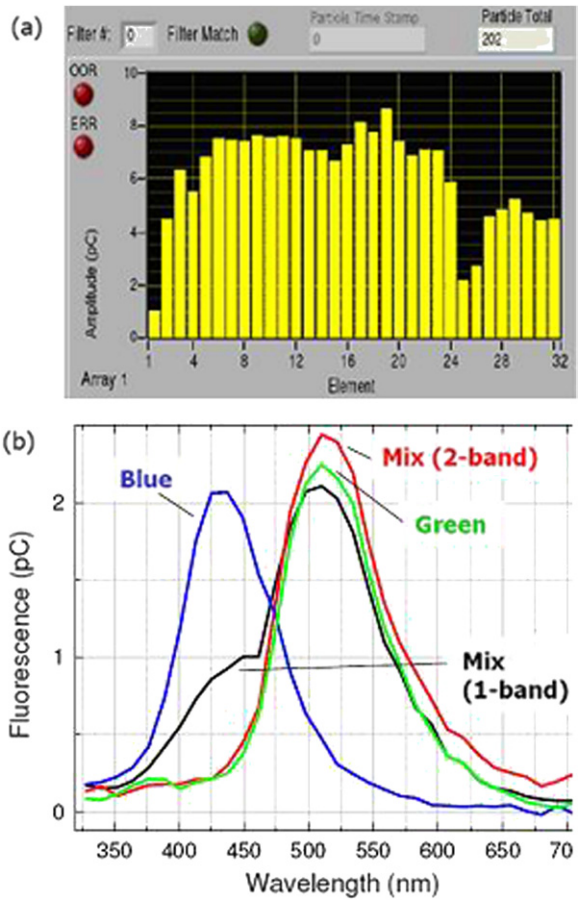

Figure 16. (*a*) Portion of PC display during data acquisition showing scatter intensity detected per LED element, and (*b*) fluorescence spectra averaged over flagged PSL particles.

eliminate the possibility of highly fluorescent blue particles, or clusters, from tripping the green flag. The system collects not only fluorescence spectra but also scatter intensities and LED illumination intensities, all in real time. Both optical hardware and present electronics acquire these optical signals, and the design of more sophisticated algorithms targeted to bio-aerosol fluorescence using these data is under development. Application and testing of new algorithms is enabled by the reprogrammable nature of the DSP.

Results of the algorithm were used to trigger the mini-aerodynamic deflector located downstream from the LED array illumination, a distance corresponding to approximately 6 ms after the particle entered the optical system. Figure 17 is an epi-fluorescence image of the deflected and undeflected aggregates of spheres in the case where green PSLs were selected using the two-band algorithm. In this configuration, the area containing deflected particles is smaller than 250 μm in diameter. Among 5000 doped water droplets, 185 were flagged as having green fluorescence. Counting deflected particles yields nominally 180 green and 8 mistakenly removed blue ones. The particle generation rate was such that successive water droplets were well separated in space and hence unaffected by gas bursts intended for adjacent particles. Thus, deflected blue particles indicate that the algorithm targeted to green particles yielded a flag for a blue one or that clusters of multiple PSLs were present

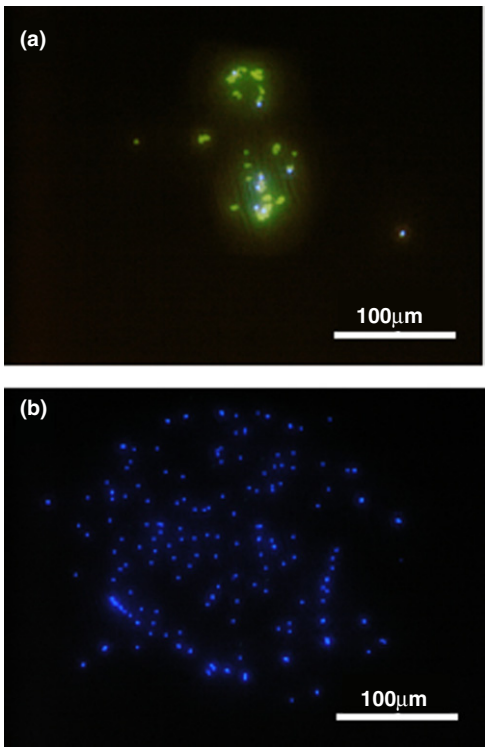

Figure 17. Epi-fluorescence images of (*a*) deflected green and (*b*) undeflected blue PSL spheres.

in a single water drop. However, undeflected particles are exclusively blue, hence no 'suspicious' (green) particles were falsely categorized as 'safe' (blue), indicating that upon receipt of a trigger the deflector is extremely reliable in removing suspect particles from the jetstream. Thus, an improvement in the particle concentration ratio may be achieved with refined algorithms.

3.3. Conclusion

In summary, by replacing all the fundamental components with smaller and potentially more cost-effective alternatives, we have demonstrated the capability of a genuinely portable aerosol particle sensor to perform tasks that are traditionally the realm of tabletop size systems. Application of emerging UV semiconductor light emitters and use of novel detector arrangements enable compaction of the core optical components. In conjunction with custom-designed real-time electronics and a miniaturized aerodynamic deflector, the entire sensor system is now significantly reduced in size while maintaining both the capability of real-time fluorescence spectral detection and analysis and physical sorting of aerosol particles. This opens the possibility of creating truly portable aerosol warning sensors or front-end sensor networks.

Acknowledgment

The authors acknowledge the contribution by a number of colleagues, including Sowmya Venkatarami (UCSD), Jung Han and collaborators (Yale), Werner Goetz (Philips Lumileds) and Noble Johnson (PARC). Research reported in this review was supported by the NSF Biophotonics program and by the US Department of Energy.

4. Summary

In this paper, we reviewed the application of nitride-based blue–green and ultraviolet microscale LED devices in various research fields of biological science and technology. Compared with the conventional bulky fluorescence lamp and expensive bench-top laser systems, microscale LED devices show an alternate way of doing cellular/molecular level biology experiments with compact inexpensive setups.

References

[1] Ozden I, Diagne M, Nurmikko A V, Han J and Takeuchi T 2001 *Phys. Status Solidi* a **188** 139
[2] Jeon C W, Kim K S and Dawson M D 2002 *Phys. Status Solidi* a **192** 325
[3] Choi H W, Jeon C W and Dawson M D 2004 *J. Cryst. Growth* **268** 527
[4] Choi H W, Jeon C W and Dawson M D 2004 *IEEE Electron Devices Lett.* **25** 277
[5] Wu S, Chhajed S, Yan L, Sun W, Shatalov M, Adivarahan V and Khan M A 2006 *Japan. J. Appl. Phys.* **45** 352
[6] Venkataramani S, Davitt K M, Zhang J, Xu H, Song Y-K, Connors B W and Nurmikko A V 2005 *IEEE J. Sel. Top. Quantum Electron* **11** 785
[7] Bullen A and Saggau P 1999 *Biophys. J.* **76** 2272
[8] Brewer G J, Torricelli J R, Evege E K and Price P J 1993 *J. Neurosci. Res.* **35** 567
[9] Kandel E R, Schwartz J H and Jessell T M 2000 *Principles of Neural Science* 4th edn (New York, NY: McGraw-Hill) pp 152–3
[10] Hamill O P, Marty A, Neher E, Sakmann B and Sigworth F J 1981 *Pfluger's Arch.* **391** 85
[11] Niu L and Hess G P 1993 *Biochemistry* **32** 3831
[12] Callaway E M and Katz L C 1993 *Proc. Natl Acad. Sci. USA* **90** 7661
[13] Denk W 1997 *J. Neurosci. Methods* **72** 39
[14] Parpura V and Haydon P G 1999 *Croat. Med. J.* **40** 340
[15] Chitnis A, Adivarahan V, Zhang J P, Wu S, Sun J, Shatalov M, Pachipulusu R, Mandavilli V, Gaevski M and Khan M A 2002 *IEEE Electron. Lett.* **25** 1709
[16] Chitnis A, Pachipulusu R, Mandavilli V, Shatalov M, Kuokstis E, Zhang J P, Adivarahan V, Wu S, Simin S and Khan M A 2002 *Appl. Phys. Lett.* **16** 2938
[17] Venkataramani S, Davitt K M, Xu H, Zhang J, Song Y-K, Connors B W and Nurmikko A V 2007 *J. Neurosci. Methods* **160** 5
[18] Ren Z *et al* 2005 *Mater. Res. Soc. Proc.* **831** 21
[19] Peng H *et al* 2004 *Appl. Phys. Lett.* **85** 1436
[20] Xu H, Davitt K M, Dong W, Song Y-K, Patterson III W R, Aizenman C D and Nurmikko A V 2008 *IEEE J. Sel. Top. Quantum Electron.* **14** 167–70
[21] Jean F, Bourg-Heckly G and Viellerobe B 2007 *Opt. Express* **15** 4008
[22] Vincent P, Charvet I, Bourgeais L, Stoppini L, Leresche N, Changeux J P, Lambert R, Meda P and Paupardin-Tritsch D 2006 *EMBO Report* vol 7 p 1154
[23] Thiberville L, Moreno-Swirc S, Vercauteren T, Peltier E, Cave C and Bourg-Heckly G 2007 *Am. J. Respir. Crit. Care Med.* **1** 22
[24] Kaye P H, Stanley W R, Hirst E, Foot E V, Baxter K L and Barrington S J 2005 *Opt. Express* **13** 3583

[25] Jeys T H, Desmarais L, Lynch E J and Ochoa J R 2003 *Proc. SPIE: Sensors, and Command, Control Communications and Intelligence Technologies for Homeland Defense and Law Enforcement II (Orlando, FL)* vol 5071 ed E M Carapezza pp 234–40

[26] Davitt K M, Song Y-K, Patterson W R III, Nurmikko A V, Gherasimova M, Han J, Pan Y L and Chang R K 2005 *Opt. Express* **13** 9548

[27] Davitt K M, Song Y-K, Patterson W R III, Nurmikko A V, Ren Z, Sun Q and Han J 2007 *Phys. Status Solidi* a **204** 2112

[28] Adivarahan V, Wu S, Sun W H, Mandavilli V, Shatalov M S, Simin G, Yang J W, Maruska H P and Khan M A 2004 *Appl. Phys. Lett.* **85** 1838